Journal of Materials Chemistry

www.rsc.org/materials

Volume 18 | Number 43 | 21 November 2008 | Pages 5169–5308

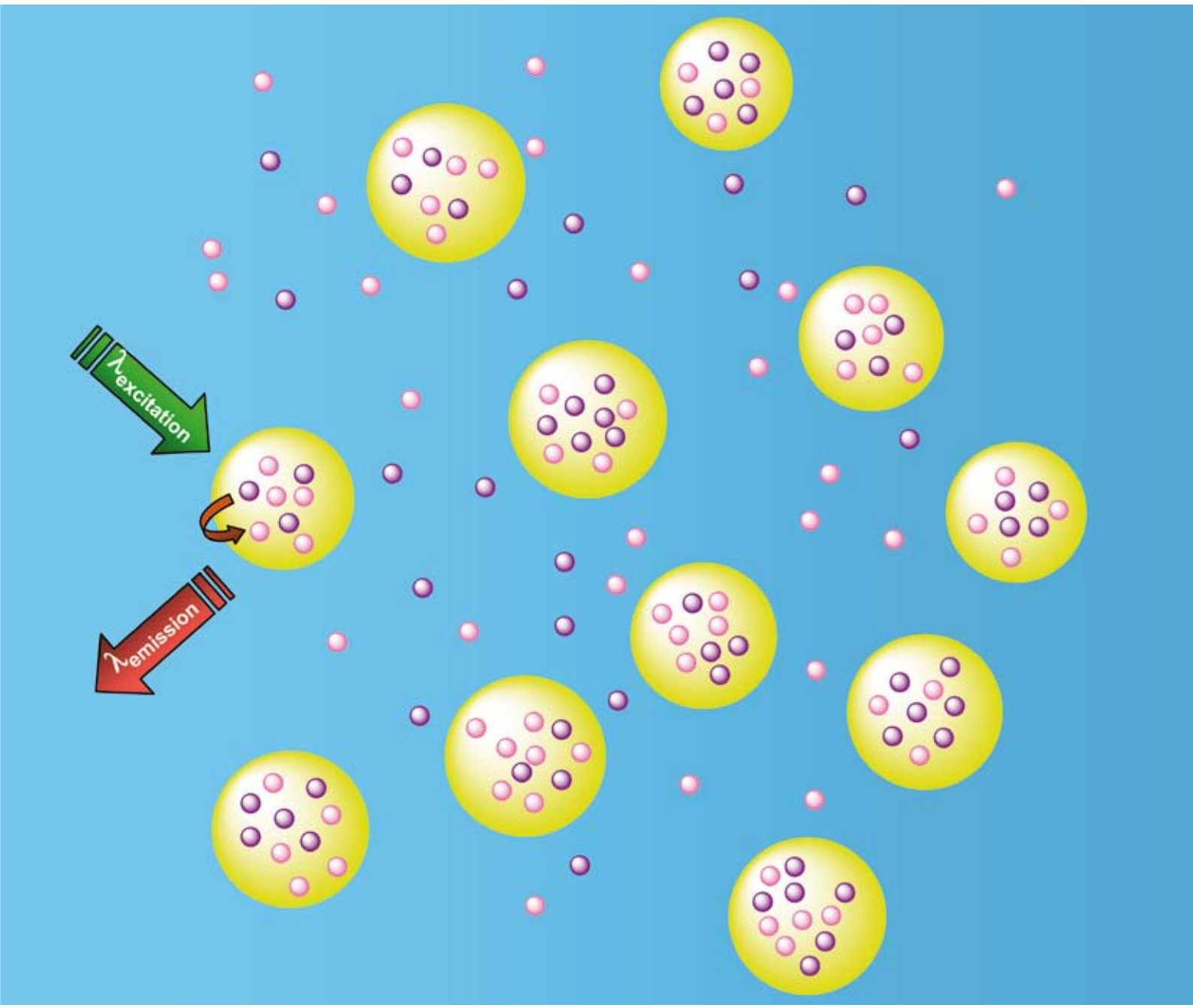

ISSN 0959-9428

RSC Publishing

0959-9428(2008)18:43;1-R

Lanthanide doped ZnS quantum dots dispersed in silica glasses: an easy one pot sol–gel synthesis for obtaining novel photonic materials†

José Planelles-Aragó,*[a] Beatriz Julián-López,*[a] Eloisa Cordoncillo,[a] Purificación Escribano,[a] Fabienne Pellé,[b] Bruno Viana[b] and Clément Sanchez[b]

Received 2nd June 2008, Accepted 13th August 2008
First published as an Advance Article on the web 3rd October 2008
DOI: 10.1039/b809254k

Silica glasses containing both ZnS quantum dots (QDs) and luminescent lanthanide ions are attractive candidates to develop new lighting displays, sensor devices or laser emitters. This work reports an easy sol–gel method to prepare Eu^{3+}-doped and Eu^{3+},Mn^{2+}-codoped ZnS nanocrystals dispersed in a transparent silica matrix. Semiconductor nanocrystals with an average size of 5–6 nm and exhibiting both cubic and hexagonal phases were obtained at low temperature. The luminescent interactions between ZnS QDs, Eu^{3+} and Mn^{2+} ions provided materials with different optical responses but also gave information about the organization of the different species in the nanocomposite. Indeed, Eu ions were found to be both dispersed within the silica and located at the surface of the nanochalcogenide, the latter providing a ZnS → Eu^{3+} energy transfer. Incorporation of Mn^{2+} into the ZnS lattice induced the appearance of defect states that enhance the blue luminescence of the nanocomposite. These results underline the sensitivity of optical processes to the nature and organization of the active species, which is of vital importance for the design of photonic materials.

Introduction

The synthesis and optical studies of inorganic and hybrid nanostructured materials have become a major interdisciplinary area of research over the past 20 years.[1,2] Semiconductor nanoparticles (NPs) play a major role in several new technologies, the intense interest in this area derives from their unique chemical, physical and electronic properties, which give rise to their potential uses in the fields of displays, lighting, sensors and lasers, as well as other areas.

Zinc sulfide (ZnS) as an important wide-bandgap (3.6 eV) semiconductor has been used as a key material for ultraviolet light-emitting diodes and injection lasers,[3] flat-panel displays,[4] electroluminescent devices and infrared windows.[5]

In recent years, some unique characteristics of ZnS nanocrystals different from bulk crystals have enlarged the range of applications. Among the wide-bandgap semiconductors, ZnS has a large exciton binding energy (40 meV) and a small Bohr radius (2.4 nm) which make it an excellent candidate for exploring the intrinsic recombination processes in dense excitonic systems.

Furthermore, ZnS nanocrystals or quantum dots, having sizes comparable to that of the bulk Bohr exciton radius, exhibit discrete electron energy levels with high oscillator strength and strong luminescence due to the well known quantum confinement effects. Thus, the study of this nanosized semiconductor is of considerable importance and great efforts have been focused on their synthesis and physical properties.[6] As one of the most important semiconductors, ZnS has been known for a long time as a versatile and excellent phosphor host material: when doped with appropriate ions, a variety of photoluminescent, cathodoluminescent,[7] electroluminescent,[8] and thermoluminescent[9] properties can be achieved. The luminescence characteristics of impurity-activated ZnS nanocrystals differ markedly from those of bulk ZnS. Yang *et al.*[10] give two reasons for this behavior: first, the high degree of dispersion in the nanocrystalline system; second, the size-dependent properties of semiconductor nanoparticles. It is well known that rare earth (RE) elements are effective luminescent centres for RE-doped semiconductors, because the excitation of the RE ions can occur by the recombination of photogenerated carriers confined in the semiconductor, and subsequent energy transfer to the RE ions.[11]

In a previous work[12] we reported the synthesis and optical study of Eu^{3+}-doped CdS nanocrystals embedded in silica matrices. Lanthanide doped CdS nanoparticles confined and randomly dispersed in highly transparent silica glasses were prepared by an easy one-pot sol–gel methodology that provides excellent optical properties.[13] An accurate spectroscopic study revealed the existence of energy transfer processes between CdS nanocrystals and europium ions when these species are spatially close. However, very short distances between the active species led to back-transfer processes and a reduction of the luminescence. When CdS nanocrystals are replaced by ZnS, a more extended, useful and less toxic semiconductor, important changes in the optical properties of the material are expected. Since the ionic radius of the Cd^{2+} ion is larger than that of the

[a]*Departamento de Química Inorgánica y Orgánica, ESTCE, Universitat Jaume I, 12071, Castellón, Spain. E-mail: jplanell@qio.uji.es; julian@qio.uji.es.; Fax: +34 964 728214; Tel: +34 964 728234*
[b]*Laboratoire de Chimie de la Matière Condensée, CNRS-UMR 7574, 75231, Paris, France. E-mail: bruno-viana@enscp.fr.; Fax: +33 146347489; Tel: +33 153737933*

† Electronic supplementary information (ESI) available: ATR-FTIR spectra of as-synthesized and fired EZS samples. See DOI: 10.1039/b809254k

Zn^{2+} ion (0.78 and 0.60 Å respectively in four-fold coordination for blende-type structures),[14] it is expected that Eu^{3+} ions (with an ionic radius of 1.07 Å for eight-fold coordination) are not able to be incorporated in the ZnS network and could be located at the nanoparticle surface. In this situation, the ZnS → Eu^{3+} energy transfer could be more efficient (*i.e.* Eu^{3+} ions are incorporated more easily in CdS than in ZnS and therefore a weaker Eu^{3+} → ZnS back-transfer process should occur). Furthermore, in order to facilitate energy transfer to Eu^{3+} centers upon excitation of the ZnS host, Mn^{2+} ions can be introduced in these materials. Mn-doped ZnS nanocrystals have been widely studied[9] showing a good degree of Mn^{2+} incorporation in the ZnS host and an efficient ZnS → Mn^{2+} energy transfer phenomenon that gives rise to a characteristic orange luminescence attributed to the spin forbidden electronic transition of Mn^{2+} ions in a tetrahedral site. On the other hand, efficient Mn^{2+} → Ln^{3+} energy transfer processes (where Ln^{3+} is a lanthanide ion) have been observed in a variety of rare-earth doped Mn containing crystals such as MnF_2 and $RbMnF_3$.[15] Due to the similar energies of the transitions $^4T_1 \rightarrow {}^6A_1$ of Mn^{2+} and $^5D_0 \rightarrow {}^7F_J$ ($J = 0$–6) of Eu^{3+} ions (see Fig. 1), an energy transfer Mn^{2+} → Eu^{3+} is expected when ZnS NPs are excited.

This work presents the structural and optical study of Eu^{3+}-doped and Eu^{3+},Mn^{2+}-codoped ZnS nanoparticles trapped in an amorphous and transparent silica matrix. These multicomponent nanomaterials have been prepared by a one pot sol–gel technique, where nanocrystals are generated by thermal treatment. Structural characterization of the nanocomposites is performed by high resolution transmission electron microscopy (HRTEM). The optical features of each system, as well as energy transfer between semiconductor nanoparticles and the doping ions, are analyzed by UV-visible spectrophotometry, excitation and emission spectra and time-resolved luminescence.

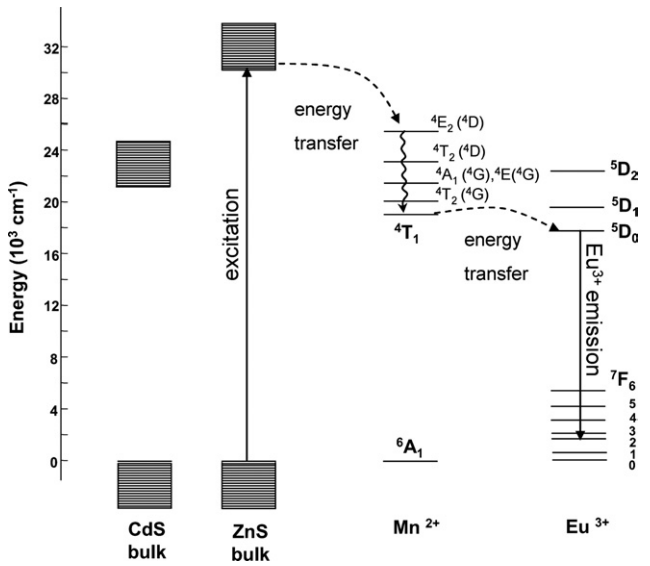

Fig. 1 Optical mechanism suggested for Eu^{3+},Mn^{2+}-codoped ZnS nanocrystals. The Mn^{2+} ions provide energy transfer to Eu^{3+} centers upon excitation of ZnS nanocrystals.

Experimental

Sample preparation

Highly transparent and colorless silica monoliths containing Eu^{3+}-doped and Eu^{3+},Mn^{2+}-codoped ZnS nanoparticles were prepared using a modification of a previously reported sol–gel methodology.[12,13] In our procedure ZnS nanocrystals are generated by decomposition of Zn^{2+}-DMSO (DMSO = dimethylsulfoxide) complexes formed in solution and their growth is restricted by the sol–gel silica medium avoiding undesired particle aggregation processes. The role of DMSO is two-fold: it acts as a solvent and as a sulfur source, thus avoiding the use of H_2S in the synthesis of ZnS. After a mild heat treatment, highly transparent glasses containing crystalline Eu^{3+}-doped ZnS and Eu^{3+},Mn^{2+}-codoped nanoparticles are obtained providing interesting optical properties.

The Eu^{3+}-doped ZnS sample, labelled as EZS, is prepared as follows: solutions of zinc nitrate ($Zn(NO_3)_2 \cdot 6H_2O$, 98%, Strem) and europium nitrate ($Eu(NO_3)_3 \cdot 6H_2O$, 99.9%, Strem), dissolved in the minimum amount of DMSO (dimethyl sulfoxide, $(CH_3)_2SO$, Panreac), are mixed and left stirring for 30 min. The resulting solution is added to a mixture of TEOS (tetraethoxysilane, ($Si(OC_2H_5)_4$, Strem, 99%), DMSO, and water to obtain a molar composition of 1 TEOS : 44.4 DMSO : 0.025 Zn(II) : 7.182×10^{-3} Eu(III) : 10.5 H_2O. After stirring for 30 min at room temperature, the resulting solution is heated at 80 °C for a week. Finally, different amounts of the final sol are poured into vessels and allowed to dry by means of infrared lamps. After drying, transparent and colorless xerogels are fired in a furnace at 500 °C for 30 min with a heating rate of 5 °C min^{-1}. This treatment was chosen according to the results of differential thermal analysis and thermogravimetry.

The Eu^{3+},Mn^{2+}-codoped ZnS sample, labelled as EMZS, is prepared as described for the EZS sample, but using manganese(II) acetylacetonate ($Mn(CH_3COCHC(O)CH_3)_2$, 95%, Strem) as Mn^{2+} precursor. The resulting molar composition of EMZS sample is 1 TEOS : 44.4 DMSO : 0.025 Zn(II) : 8.587×10^{-3} Mn(II) : 3.591×10^{-3} Eu(III) : 10.5 H_2O. As references for optical measurements, non-doped ZnS nanoparticles in SiO_2 (ZS), Eu^{3+}-doped SiO_2 (ES) and pure SiO_2 (S) samples were also prepared following the same experimental procedure.

Characterization techniques

The characterization by high resolution transmission electron microscopy (HRTEM) was carried out on a Philips CM20 (200 kV) microscope (CME, Orleans University, France). For this analysis, the ground samples were dispersed in ethanol and a drop was deposited onto a carbon-coated copper grid.

The chemical compositions of the materials were determined by X-ray fluorescence (XRF) measurements using a Siemens SRS 3000 wavelength dispersive XRF spectrophotometer.

Absorption spectra were recorded in a Cary 5 Varian spectrophotometer using an attenuator in order to avoid saturation of the absorption signal. Excitation and emission spectra were recorded using an Eclipse (Varian) spectrofluorimeter, containing a Xe lamp source. Time-resolved luminescence measurements were performed with $\lambda_{exc} = 280$ nm and $\lambda_{em} = 617$ nm ($^5D_0$ decay) and lifetime values were extracted from decay

profiles. All optical measurements were carried out at room temperature.

The Fourier transform infrared (FTIR) spectra were recorded between 4000 and 400 cm^{-1} (resolution of 4 cm^{-1}) on a Equinox 55 Bruker spectrometer (ESI†). The spectra were obtained on bulk samples using an ATR (attenuated total reflection) instrument equipped with a ZnSe monocrystal. The advantage of measuring with the ATR device is to detect the presence of hydroxyl groups inside the sol–gel material.

Results and discussion

Microstructural characterization

The first characterization of the EZS and EMZS samples was performed by X-ray diffraction. The patterns of raw and fired monoliths exhibited the typical vitreous halo characteristic of the amorphous silica matrix. In order to observe nanocrystallization inside the amorphous silica glass we used high resolution transmission electron microscopy (HRTEM). HRTEM micrographs evidence the crystalline nature of the nanoaggregates in annealed samples. Fig. 2 shows a typical spherical 6 nm ZnS particle embedded in the amorphous silica medium. The selected area electron diffraction (SAED) pattern of these nanocrystallites is shown in the inset of Fig. 2. As expected, in the case of nanocrystals, the electron diffraction pattern shows a set of rings instead of spots due to the random orientation of the nanocrystallites, corresponding to the diffraction from different atomic planes of the nanocrystallites.[16]

Higher magnification TEM pictures of individual crystallites were recorded in order to resolve the lattice planes. The *d* interplanar distances obtained from the HRTEM micrographs, and shown in Table 1, are similar to those included in JCPDS files for cubic and hexagonal ZnS polymorphs (JCPDS: 5-566 and 79-2204). These data suggest that for the nanometer-sized particles of ZnS, the equilibrium temperature for the cubic-to-hexagonal transition is significantly reduced from the bulk value.[17] Therefore, we can find both ZnS phases coexisting in our samples. This result is consistent with the observations of Goldstein *et al.*[18] who observed the melting temperature of nanoparticles of CdS to be substantially reduced over the bulk value.

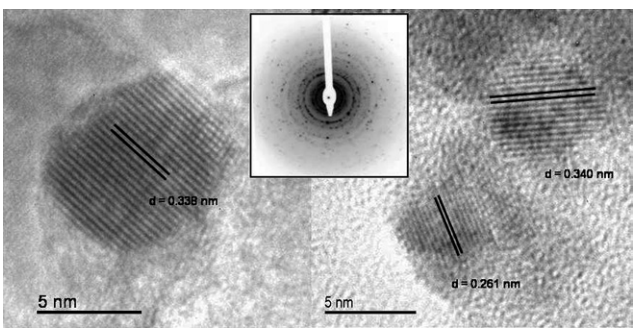

Fig. 2 HRTEM micrographs and EDX pattern (inset) of EZS sample after firing at 500 °C.

Table 1 *d*-Spacing of the crystalline ZnS NPs measured from HRTEM micrographs

d-Spacing/Å	(*hkl*) values	Phase assignment
3.3	(100)	hexagonal
3.1	(002)/(111)	hexagonal/cubic
2.6	(200)	cubic

Table 2 Chemical compositions of EZS and EMZS samples

	Si	Zn	Mn	Eu
EMZS	92.0573%	5.6779%	1.3301%	0.9347%
EZS	92.4897%	5.6691%	—	1.8412%

Energy dispersive X-ray (EDX) analyses were performed in order to determine the composition of the aggregates but their size was smaller than that of the detection area and no reliable conclusions could be extracted. No information about doping ions localization (both Eu^{3+} and Mn^{2+} ions) could be obtained because of the low molar percentage of these elements in our samples. However, XRF analysis will shed some light on the content of these ions within the material. Table 2 details the chemical compositions of EZS and EMZS samples determined by XRF measurements. One can see from the XRF data that the Zn, Eu and Mn contents are very close to those in the precursor DMSO solutions.

UV-Visible spectroscopy

The UV-visible absorption spectra of annealed samples are illustrated in Fig. 3. The spectrum of the reference S sample (pure silica) reveals the good optical quality of the glasses since it is completely transparent in the 250–700 nm range. Upon incorporating ZnS nanoparticles into the silica matrix (ZS), the resulting spectrum shows an absorption edge at ~314 nm (3.95 eV, value obtained from the first derivative method used to determine the edge position in all samples). The corresponding bandgap energy for the ZnS nanocrystallites is larger than that observed in bulk ZnS (3.7 eV, 335 nm). This blue shift toward higher energy can be explained as a quantum size effect, due to the electron–hole confinement in a small volume.[19] Indeed,

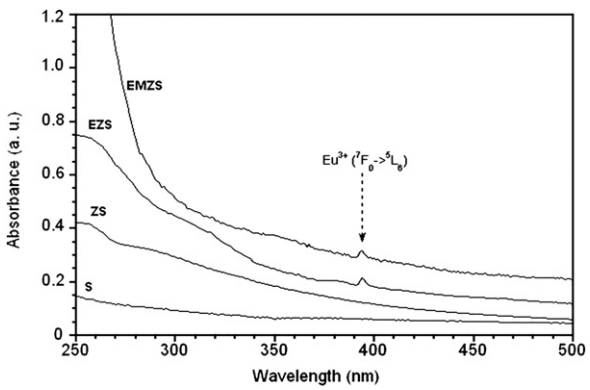

Fig. 3 UV-Visible optical absorption spectra of Eu^{3+}-doped and Eu^{3+},Mn^{2+}-codoped ZnS samples, EZS and EMZS respectively. As references, non-doped ZnS nanoparticles in SiO_2 (ZS) and silica matrix (S) absorption spectra have been included. The acronym a.u. in the *y* axis refers to absorbance units.

particle sizes of ZnS were found to be around 5 nm, according to a calibration curve presented by Rossetti *et al.*[20] This curve following the Brus model is based on variational calculations of the cubic ZnS lowest excited state energy as a function of nanoparticle diameter.[21] These particle size calculations are in good agreement with our HRTEM observations.

Regarding ZnS nanocrystals in EZS and EMZS samples, they exhibit similar absorption edges to the ZS sample. These profiles are also analogous to those corresponding to Eu^{3+}-doped ZnS nanoparticles obtained by other synthesis methods and reported previously.[22] Some studies indicate that addition of the doping ions cannot change the average size of the nanocrystals,[23] but it can increase the size distribution significantly, modifying the shape of absorption curves. In our curves, only slight contributions due to the presence of Eu^{3+} and Mn^{2+} doping ions can be observed. The presence of Eu^{3+} ions increases the absorption intensity in the UV region, which can be attributed to the Eu–O charge transfer. Furthermore, absorption bands corresponding to the forbidden 4f–4f transitions are usually weak and only a small absorption located at 394 nm is detected and attributed to the $^7F_0 \rightarrow {}^5L_6$ transition.[7]

Photoluminescence: excitation

Photoluminescence excitation spectra of annealed Eu^{3+} containing samples (ES, EZS and EMZS) performed monitoring the $^5D_0 \rightarrow {}^7F_2$ transition (615 nm) are presented in Fig. 4. For the ES sample, the excitation spectrum exhibits the bands associated with the Eu^{3+} 4f–4f transitions at 362 nm ($^7F_1 \rightarrow {}^5D_4$), 380 nm ($^7F_0 \rightarrow {}^5G_3$), 394 nm ($^7F_0 \rightarrow {}^5L_6$), 414 nm ($^7F_0 \rightarrow {}^5D_3$), 465 nm ($^7F_0 \rightarrow {}^5D_2$), 526 nm ($^7F_0 \rightarrow {}^5D_1$) and 534 nm ($^7F_1 \rightarrow {}^5D_1$). If ZnS nanocrystals are present and spatially close to Eu^{3+} ions, an energy transfer from semiconductor nanoparticles to Eu^{3+} centers should be expected according to our previous studies on Eu^{3+}-doped CdS nanocrystals.[12] The excitation spectrum of the Eu^{3+} emission suggests the existence of ZnS $\rightarrow$ Eu^{3+} energy transfer process in Eu^{3+}-doped ZnS samples. Thus, when the ZnS absorption band is present in the excitation spectrum ZnS $\rightarrow$ Eu^{3+} transfer occurs. Although the excitation spectrum of the Eu^{3+}-doped ZnS sample (EZS) is dominated by the intra-configurational 4f–4f transitions, it shows a slight ZnS excitation band in the range 250–350 nm showing an inefficient ZnS–Eu^{3+} energy transfer. Due to the poor incorporation of Eu^{3+} ions in nanocrystalline ZnS, the interaction between ZnS nanoparticles and Eu^{3+} ions is indeed expected to be weak. There are several reasons for the problematic incorporation of lanthanide ions in ZnS nanocrystallites.[24] First, the ionic radius of the lanthanide ions is generally larger than that of Zn^{2+} ions (Eu^{3+} and Zn^{2+} radii are 0.95 and 0.74 Å respectively for coordination number 6).[14] For a Eu^{3+} ion on a Zn^{2+} lattice site, the ZnS lattice should be strongly distorted, which is energetically unfavourable. Besides, due to the large ionic radius, Eu^{3+} cations indeed prefer high coordination number sites (typically six or higher). In ZnS, however, the coordination number of the cation lattice site is only four, which is very unfavorable for Eu^{3+}. In addition, the trivalent charge of the Eu ion has to be compensated in the lattice, so it is therefore questionable if trivalent europium can be incorporated in a sulfide compound. A divalent state is expected to be more suitable in terms of charge but the Eu^{2+} size prevents the insertion (1.17 Å for coordination number 6).[14]

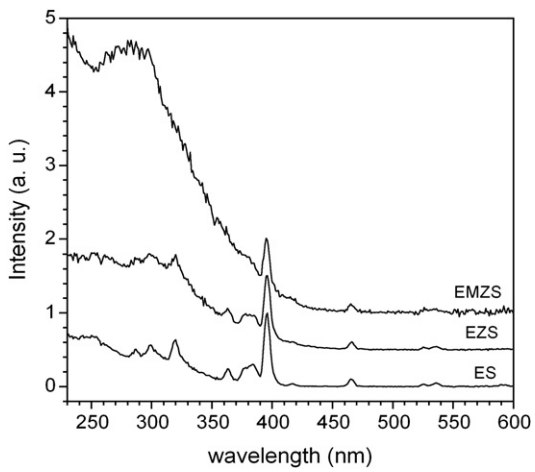

Fig. 4 Excitation spectra of Eu^{3+}-doped and Eu^{3+},Mn^{2+}-codoped ZnS samples, EZS and EMZS respectively, the emission of Eu^{3+} was monitored at 615 nm ($^5D_0 \rightarrow {}^7F_2$ transition). As a reference, the Eu^{3+}-doped SiO_2 (ES) spectrum has been included. Spectra have been normalized to the 394 nm band and then shifted along the *y*-axis (in arbitrary units, a.u.) with the aim of facilitating their visibility.

In order to improve the interaction between ZnS nanoparticles and Eu^{3+} centers, Mn^{2+} was introduced in our samples. Mn^{2+} is more easily incorporated in the ZnS lattice and efficient ZnS $\rightarrow$ Mn^{2+} energy transfer has been demonstrated previously.[11] As shown in Fig. 4, the excitation spectrum of the EMZS sample indicates a more efficient ZnS $\rightarrow$ Eu^{3+} energy transfer phenomenon.

In this spectrum, Eu^{3+} excitation bands are drastically reduced in intensity in comparison to the broad absorption band clearly observed below 350 nm. These results could be attributed to an energy transfer from ZnS particles to Eu^{3+} centers. The proposed mechanism for this transfer process, in the presence of Mn^{2+}, can be illustrated as shown in Fig. 1. In the process, upon ZnS excitation, the energy can be transferred from ZnS to Mn^{2+} and these ions, in turn, can transfer to Eu^{3+} centers, giving rise to the characteristic $^5D_0 \rightarrow {}^7F_2$ emission (transition targeted in the excitation spectra). We suggest that this $Mn^{2+} \rightarrow Eu^{3+}$ transfer can occur due to the closeness between the excited states $^4T_1$ and $^5D_0$ corresponding to Mn^{2+} and Eu^{3+}, respectively.

Photoluminescence: emission

Emission spectra of the samples were recorded upon excitation at 280 nm, which corresponds to the semiconductor absorption onset detected in the UV-visible spectra, in order to study the energetic interaction between ZnS nanocrystals and Eu^{3+} and Mn^{2+} doping ions. Fig. 5 depicts the luminescence spectra recorded for the samples EZS and EMZS together with those of the references ES and ZS, after annealing at 500 °C. They have been normalized to the host independent band located at ~590 nm (parity-allowed magnetic dipole $^5D_0 \rightarrow {}^7F_1$ transition) with the aim of comparing the relative intensities of the bands.

The features of Eu^{3+} radiative relaxation in Eu-doped silica glass are first studied from the emission spectrum of the reference ES (in grey). It exhibits the main emission bands characteristic of

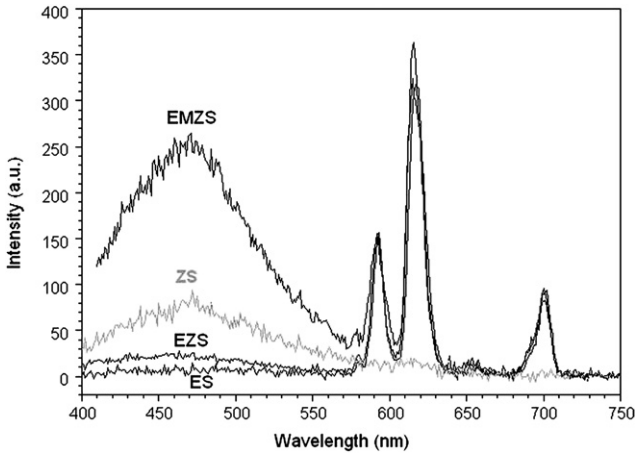

Fig. 5 Emission spectra of Eu^{3+}-doped (EZS) and Eu^{3+},Mn^{2+}-codoped (EZMS) ZnS–SiO_2 samples, together with those of Eu^{3+}-doped SiO_2 (ES) and ZnS–SiO_2 (ZS) references, annealed at 500 °C upon excitation at 280 nm. They are normalized according to the host independent $^5D_0 \rightarrow {}^7F_1$ emission (590 nm). The intensity scale of the ZS spectrum has been multiplied in order to stand out the large emission band centred at 475 nm. The acronym a.u. in the *y* axis refers to arbitrary units.

the transitions from the $^5D_0$ levels to the ^7F_J multiplets ($J = 0$, 1, 2, 3 and 4) at 579, 593, 617, 656 and 701 nm, respectively. The broadening of the bands indicates that Eu^{3+} ions are distributed in different environments. This behaviour, usually found in lanthanide-doped glasses,[25–27] is explained by the inhomogeneous dispersion of the active centres within the amorphous silica matrix as a consequence of its low solubility (the ionic radii of Si^{4+} and Eu^{3+} are 0.26 Å and 1.07 Å respectively for their typical coordination numbers 4 and 8).[14] Actually, europium species are expected to be aggregated in small clusters randomly distributed within the silica glass.

On the other hand, the spectrum (shown in Fig. 5) of the reference ZS sample shows a broad blue emission at 470 nm. For most semiconductor nanocrystals, emission bands related to excitonic luminescence and to impurities/defects luminescence can appear in the fluorescence spectrum. Since the former are sharp and located at the absorption edge, we can attribute the detected blue emission to the electron–hole recombination through shallow surface trap states of ZnS nanocrystals with lattice defects.[28]

When the compounds are doped with Eu^{3+} ions (EZS), both contributions from Eu ions and ZnS nanocrystals are detected in the emission spectrum. Both radiative paths for energy relaxation are observed, but lanthanide emission is predominant. The low intensity of the surface state emission suggests a low defect density in ZnS nanoparticles, similar to that observed for the ZS sample (note that on Fig. 5 the emission spectrum of ZS has been amplified). This fact indicates that the presence of Eu-doping ions in the sol–gel synthesis does not affect significantly the processes of nucleation and growth of ZnS nanocrystals within the silica matrix. Another interesting feature in the spectrum is the broadness exhibited by the Eu^{3+} emission peaks, revealing different surroundings for lanthanide cations. Going deeper in this topic, we analysed the ratio between the areas of the "hypersensitive" electric $^5D_0 \rightarrow {}^7F_2$ and the magnetic dipolar $^5D_0 \rightarrow {}^7F_1$ transitions, which is considered as a parameter to measure the "asymmetry" in the vicinity of Eu^{3+} ions and Eu–O covalency. It has been established that this ratio increases when the lattice environment is distorted due to the odd parity crystal field parameters. After deconvolution of the spectra, we found that the asymmetry parameter for EZS is slightly higher than for ES ($ratio_{EZS} = 3.2$, $ratio_{ES} = 2.7$). These values well agree with those typically found in sol–gel derived materials.[29–31] However, the difference can be associated to the change in chemical surroundings of Eu^{3+} in different media. If we bear in mind that Eu ions cannot enter the ZnS lattice and substitute for the Zn^{2+} ions, the more distorted local environment of Eu sites as well as the more covalent Eu–O bond in EZS can be related to some interaction of Eu^{3+} ions with ZnS nanoparticles, which must be spatially close. This proximity also explains the possibility of ZnS $\rightarrow$ Eu^{3+} energy transfer detected in excitation spectra. However, it is very difficult to know exactly the Eu location and the extent of this interaction (chemically or physically adsorbed at the surface, co-occupying the zenith of the ZnS lattice by the multi-ZnS crystals, *etc.*).

The activation of the nanocomposite with Mn^{2+} ions (sample EMZS) leads to a significant increase of the blue emission (13 times more intense than in EZS) in comparison to the Eu^{3+} emission. The first conclusion is that the extent of lattice defects in ZnS nanocrystals is much higher than in EZS and ZS. The intensity of the radiative emission from defects is consistent with the formation of a solid solution Mn^{2+}:ZnS, since Mn^{2+} ions with a ionic radius 10% larger than Zn^{2+} would be occupying Zn positions and creating distortions in the crystalline structure.[32–34] In this sample, Eu^{3+} ions would be, as well, spatially close to Mn:ZnS nanocrystals because of the Mn:ZnS $\rightarrow$ Eu^{3+} energy transfer detected in the excitation spectrum, however the main energy relaxation pathway is through defect center emission. Mn^{2+} luminescence in Mn-doped materials should present a characteristic red emission at around 590 nm which is not observed here. It is reported that the emission intensity decreases when the Mn^{2+} concentration increases.[35] The absence of Mn^{2+} emission in the present compounds suggests high local concentrations of Mn^{2+} ions in the nanocrystals, which is expected due to their small size. Due to the low loading of Mn^{2+} ions in these materials, uniform doping of ZnS nanoparticles might be difficult. It is likely that only a fraction of the ZnS nanocrystals would actually be doped or in contact with Eu^{3+} or Mn^{2+}. In the case of the EMZS sample, mixed regions could exist in combination with others rich in Eu^{3+} or in Mn^{2+} ions. Another possibility would be the existence of an efficient $Mn^{2+} \rightarrow Eu^{3+}$ energy transfer because of the good resonance between the energy corresponding to the $^4T_1 \rightarrow {}^6A_1$ (Mn^{2+}) and $^5D_0 \rightarrow {}^7F_J$ (Eu^{3+}) transitions. This transfer should enhance the Eu photoluminescence, but this is not the case, even if we can notice some reduction of the emission (not visible in Fig. 5 because of the normalization). This result is not surprising since the reduction of luminescence in highly defective structures has already been pointed out by Sun *et al.*.[22] A possible explanation for this quenching could be that the presence of Mn^{2+} produce a significant surface modification and crystal defects acting as recombination centers, which increase the non-radiative relaxation paths. These observations underline the potential of optical measurements to give structural information that is difficult to be identify

by HRTEM for instance. Regarding the asymmetry parameter, the deconvolution of the EMZS spectrum gave a ratio of 2.6. This value which is close to the ES one reveals a more symmetric vicinity of Eu^{3+} ions than in the EZS sample, and may be associated to a higher number of Eu^{3+} ions inside Eu aggregates. This effect is certainly due to the presence of Mn which hinders the interaction between Eu ions and ZnS crystals.

Time resolved luminescence

Fluorescence decay profiles were measured monitoring the Eu^{3+} $^5D_0 \rightarrow {}^7F_2$ transition at 617 nm. Decay curves display non-single exponential behaviour. This could be attributed to the strong disorder for Eu surroundings (Eu aggregates). This agrees well with the inhomogeneous broadening of the emission bands. Mean lifetime values were calculated using the equation:

$$\tau = \frac{\int_{t_0}^{t_1} I(t) t \mathrm{d}t}{\int_{t_0}^{t_1} I(t) \mathrm{d}t}$$

where $t_0 = 0$ and t_1 is the time where the luminescence intensity reaches the background. The lifetime values are reported in Table 3.

Lifetime values vary between 435 and 511 μs before annealing, in accordance with other similar Eu-doped sol–gel glasses.[36–38] One can notice a reduction of the lifetime values after thermal treatment which is in contrast to the usual results in case of Eu-doped silica compounds. To explain this behavior, different factors must be analyzed. The first parameter that usually plays an important role in the decay rate is the presence of CH– and OH– groups in the Eu^{3+} environment. These groups are well-known quenchers of the luminescence[39] since they absorb near Eu emission, favouring non-radiative relaxation phenomena. The heat treatment should reduce these groups, providing longer lifetime values, but this behaviour does not agree with the experimental results. FTIR measurements have been performed in order to verify the absence of OH and CH groups (see ESI†). Therefore, another parameter dominates the deexcitation processes in our samples: the dispersion/aggregation degree of active ions. It is known that, even with low doping content, a high local concentration of Eu ions facilitates the non-radiative processes. Thus, the values in Table 3 indicate some extent of Eu aggregation in the three samples (EZS, EMZS and ES). This point was previously suggested from emission spectra. Furthermore, the decrease of the values with temperature corresponds to the migration of the active ions towards a more stable coordination. Since lanthanide ions require high coordination numbers, the better accommodation in $ZnS–SiO_2$ materials is to be segregated as nano-oxodomains. Thus, Eu clustering has been evidenced from emission decay measurements, but probably there are still some dispersed europium ions which can interact with ZnS nanocrystals, as shown in the excitation and emission spectra. Therefore, the optical behavior depends not only on the active elements concentration in nanocomposites, but most probably on their distribution within the media also. These points are key parameters to design efficient photonic materials.

Table 3 Lifetime values of the samples before and after annealing

	τ/μs		
	EZS	EMZS	ES
Before annealing	435	435	511
After annealing	291	342	284

Conclusions

This work reports an easy sol–gel method to prepare Eu^{3+}-doped and Eu^{3+},Mn^{2+}-codoped ZnS nanocrystals dispersed in a transparent and amorphous silica matrix. Structural characterization showed that nanocrystals, with average diameters of 6 nm, exhibit both cubic and hexagonal ZnS phases. The reduction of the cubic-to-hexagonal transition temperature can be due to quantum confinement effects, as evidenced in the UV-visible absorption spectra. Combination of excitation, emission and time-resolved decay measurements allowed us to explain the luminescent interactions between ZnS nanocrystals, Eu^{3+} and Mn^{2+} ions, and provided information about the distribution of the different species in the nanocomposite. Eu cannot enter the ZnS lattice but the ZnS $\rightarrow$ Eu^{3+} energy transfer is demonstrated, indicating spatial proximity. Indeed Eu^{3+} is likely located at the surface of the nanochalcogenide. Incorporation of Mn^{2+} in the system distorts the ZnS lattice, generating a large number of defect states that enhances the blue luminescence of the nanocomposite. The existence of Eu segregated domains was also evidenced by fluorescence decay measurements. These results underline the sensitivity of optical processes to the structure of the nanocomposite and surface defects. Therefore, the control of the active ions location is of vital importance for the design of photonic materials.

Acknowledgements

This research was supported by the Spanish Government (MEC: MAT-2005-00541) and Bancaixa Foundation-Universitat Jaume I (P1 1B2007-47) projects. J. Planelles and B. Julián specially thank MEC for their PhD fellowship and "Ramon y Cajal" program, respectively.

References

1 P. Escribano, B. Julián-López, J. Planelles-Aragó, E. Cordoncillo, B. Viana and C. Sanchez, *J. Mater. Chem.*, 2008, **18**, 23.
2 Special Issue on Photonic Crystals: *Adv. Mater.*, 2001, **13**, 369.
3 T. Yamamoto, S. Kishimoto and S. Ilida, *Physica B*, 2001, **308**, 916.
4 M. Bredol and J. Merikhi, *J. Mater. Sci.*, 1998, **33**, 471.
5 R. Vacassy, S. M. Scholz, J. Dutta, H. Hofmann, C. J. G. Plummer, G. Carrot, J. Hilborn and M. Akine, *Mater. Res. Soc. Symp. Proc.*, 1998, **501**, 369; P. Calandra, M. Goffredi and V. T. Liveri, *Colloids Surf., A*, 1999, **160**, 9.
6 Y. Jiang, X. M. Meng, J. Liu, Z. Y. Xie, C. S. Lee and S. T. Lee, *Adv. Mater.*, 2003, **15**, 323; C. Ma, D. Moore, J. Li and Z. L. Wang, *Adv. Mater.*, 2003, **15**, 228; Z. W. Wang, L. L. Daemen, Y. S. Zhao, C. S. Zha, R. T. Downs, X. D. Wang, Z. L. Wang and R. J. Hemley, *Nat. Mater.*, 2005, **4**, 922; Y. F. Hao, G. W. Meng, Z. L. Wang, C. H. Ye and L. D. Zhang, *Nano Lett.*, 2006, **6**, 1650.
7 L. Ozawa, *Cathodoluminescence: Theory and Applications*, Kodansha, VCH, Tokyo, Weinheim, 1990; *Phosphor Handbook*, ed. S. Shionoya and W. M. Yen, CRC, Boca Raton, FL, 1999.
8 J. Valenta, D. Guennani, A. Manar, B. Honerlage, T. Cloitre and R. L. Aulombard, *Solid State Commun.*, 1996, **98**, 695; Y. Yamada,

T. Yamamoto, S. Nakamura, T. Taguchi, F. Sasaki, S. Kobayashi and T. Tani, *Appl. Phys. Lett.*, 1996, **69**, 88.
9 W. Chen, Z. G. Wang, Z. J. Yin and L. Y. Lin, *Appl. Phys. Lett.*, 1997, **70**, 1465.
10 P. Yang, M. K. Lü, D. R. Yuan, C. F. Song, S. W. Liu and X. F. Cheng, *Opt. Mater.*, 2003, **24**, 497.
11 R. Bhargava and R. Gallagher, *Phys. Rev. Lett.*, 1994, **72**, 416; W. Q. Peng, S. C. Qu, G. W. Cong, X. Q. Zhang and Z. G. Wang, *J. Cryst. Growth*, 2005, **282**, 179; S. Arora and S. Sundar, *Solid State Commun.*, 2007, **144**, 319; G. Ehrhart, B. Capoen, O. Robbe, F. Beclin, Ph. Boy, S. Turrell and M. Bouazaoui, *Opt. Mater.*, 2008, **30**, 1595.
12 B. Julián, J. Planelles-Aragó, E. Cordoncillo, P. Escribano, P. Aschehoug, C. Sanchez, B. Viana and F. Pellé, *J. Mater. Chem.*, 2006, **16**, 4612.
13 E. Cordoncillo, P. Escribano, G. Monrós, M. A. Tena, V. Orera and J. Carda, *J. Solid State Chem.*, 1995, **118**, 1; E. Cordoncillo, J. Carda, M. A. Tena, G. Monros and P. Escribano, *J. Sol–Gel Sci. Technol.*, 1997, **8**, 1043.
14 *Handbook of Chemistry and Physics*, ed. D. R. Lide, CRC, Boca Raton, FL, 2007.
15 B. Di Bartolo, J. Danko and D. Pacheco, *Phys. Rev. B*, 1987, **35**, 6386.
16 J. Nanda, S. Sapra, D. D. Sarma, N. Chandrasekharan and G. Hodes, *Chem. Mater.*, 2000, **12**, 1018.
17 S. B. Qadri, E. F. Skelton, D. Hsu, A. D. Dinsmore, J. Yang, H. F. Gray and B. R. Ratna, *Phys. Rev. B*, 1999, **60**, 9191.
18 A. N. Goldstein, C. M. Echer and A. P. Alivisatos, *Science*, 1992, **256**, 1425.
19 R. Bhargava, D. Gallagher and T. Welker, *J. Lumin.*, 1994, **60**, 275.
20 R. Rossetti, R. Hull, J. M. Gibson and L. E. Brus, *J. Chem. Phys.*, 1985, **82**, 552.
21 L. E. Brus, *J. Chem. Phys.*, 1984, **80**, 4403.
22 L. Sun, C. Yan, C. Liu, C. Liao, D. Li and J. Yu, *J. Alloys Compd.*, 1998, **275**, 234; D. D. Papakonstantinou, J. Huang and P. Lianos, *J. Mater. Sci. Lett.*, 1998, **17**, 1571.
23 A. A. Khosravi, M. Kundu, L. Jatwa, S. K. Deshpande, U. A. Bhagwat, M. Sastry and S. K. Kulkarni, *Appl. Phys. Lett.*, 1995, **67**, 2702.
24 A. Bol, R. van Beek and A. Meijerink, *Chem. Mater.*, 2002, **14**, 1121.
25 A. Femandes, M. C. Goncalves, V. de Zea Bermudez, R. A. Ferreira, L. D. Carlos, A. Charas and J. Morgado, *J. Alloys Compd.*, 2008, **451**, 510.
26 D. Levy, R. Reisfeld and D. Avnir, *Chem. Phys. Lett.*, 1984, **109**, 593.
27 B. Julián, R. Corberán, E. Cordoncillo, P. Escribano, B. Viana and C. Sanchez, *J. Mater. Chem.*, 2004, **14**, 3337.
28 W. Chen, Z. Wang, Z. Lin and L. Lin, *J. Appl. Phys.*, 1997, **82**, 3111.
29 C. Sanchez, *Proc. SPIE–Int. Soc. Opt. Eng.*, 1990, **1328**, 40.
30 M. Nogami, T. Enomoto and T. Hayakawa, *J. Lumin.*, 2002, **97**, 147.
31 B. Julián, R. Corberán, E. Cordoncillo, P. Escribano, B. Viana and C. Sanchez, *Nanotechnology*, 2005, **16**, 2707.
32 W. Q. Peng, S. C. Qu, G. W. Cong, X. Q. Zhang and Z. G. Wang, *J. Cryst. Growth*, 2005, **282**, 179.
33 K. Sooklal, B. S. Cullum, S. M. Angel and C. J. Murphy, *J. Phys. Chem.*, 1996, **100**, 4551.
34 L. Sun, C. Yan, C. Liu, C. Liao, D. Li and J. Yu, *J. Alloys Compd.*, 1998, **275**, 234.
35 S. Kar, S. Biswas and S. Chaudhuri, *Synth. React. Inorg. Met.-Org. Nano-Met. Chem.*, 2006, **36**, 193.
36 E. Pecoraro, R. A. Sá Ferreira, C. Molina, S. J. L. Ribeiro, Y. Messsaddeq and L. D. Carlos, *J. Alloys Compd.*, 2008, **451**, 136.
37 H. You and M. Nogami, *J. Phys. Chem. B*, 2004, **108**, 12003.
38 R. Gonçalves, Y. Messaddeq and M. Atik, *Mater. Res.*, 1999, **2**, 11.
39 R. S. Meltzer, W. M. Yen, H. Zheng, S. P. Feofilov, M. J. Dejneka, B. Tissue and H. B. Yua, *J. Lumin.*, 2001, **94**, 217.